

# Temporal Conformal Prediction (TCP): A Distribution-Free Statistical and Machine Learning Framework for Adaptive Risk Forecasting

Agnideep Aich<sup>1\*</sup>, Ashit Baran Aich<sup>2</sup> and Dipak C. Jain<sup>3</sup>

<sup>1</sup> Department of Mathematics, University of Louisiana at Lafayette, Louisiana, USA.

<sup>2</sup> Department of Statistics, formerly of Presidency College, Kolkata, India.

<sup>3</sup> European President and Professor of Marketing, CEIBS, Shanghai, PR China.

## Abstract

We propose **Temporal Conformal Prediction (TCP)**, a distribution-free framework for constructing well-calibrated prediction intervals in nonstationary time series. TCP couples a modern quantile forecaster with a split-conformal calibration layer on a rolling window and, in its **TCP–RM** variant, augments the conformal threshold with a single online Robbins–Monro (RM) offset to steer coverage toward a target level in real time. We benchmark TCP against GARCH, Historical Simulation, and a *rolling* Quantile Regression (QR) baseline across equities (S&P 500), cryptocurrency (Bitcoin), and commodities (Gold). Three results are consistent across assets. *First*, rolling QR yields the *sharpest* intervals but is *materially under-calibrated* (e.g., S&P 500: 86.3% vs. 95% target). *Second*, TCP (and TCP–RM) achieves near-nominal coverage while being substantially *narrower* than Historical Simulation (e.g., S&P 500: –29% width). *Third*, the RM update improves calibration with negligible width cost. Crisis-window visualizations around March 2020 show TCP/TCP–RM expanding and then contracting their interval bands promptly as volatility spikes and recedes, with **red dots** marking days where realized returns fall outside the reported 95% interval (miscoverage). A sensitivity study confirms robustness to window size and step-size choices. Overall, TCP provides a practical, theoretically grounded solution to calibrated uncertainty quantification under distribution shift, bridging statistical inference and machine learning for risk forecasting.

**Keywords:** Temporal Conformal Prediction, Quantile Regression, Machine Learning, Statistical Learning, Value-at-Risk, Financial Time Series, Risk Management.

*MSC 2020 Subject Classification:* 62G08, 62M10, 62P05, 91G70, 68T05

## 1. INTRODUCTION

Financial risk estimation is more than a regulatory checkbox; it is foundational for market stability and investor confidence [Markowitz, 1952, J.P. Morgan/Reuters, 1996]. Yet, when markets enter turbulent regimes, traditional risk models often fall short. Early implementations of Value-at-Risk (VaR) were predominantly *parametric*, often assuming (conditional) normality [Jorion, 2007, Dowd, 1998], assumptions that can systematically understate tail risk. Coherent

---

\*Corresponding author: Agnideep Aich, [agnideep.aich1@louisiana.edu](mailto:agnideep.aich1@louisiana.edu), ORCID: [0000-0003-4432-1140](https://orcid.org/0000-0003-4432-1140)

alternatives such as Conditional Value-at-Risk (CVaR) were introduced to address some of these limitations [Rockafellar and Uryasev, 2000]. Events like the 2008 global financial crisis [Brunnermeier, 2009] and the March 2020 stock-market crash [Mazur et al., 2021] exposed the fragility of parametric assumptions, especially in the tails.

The core challenge is that financial returns violate the independent and identically distributed (i.i.d.) assumption that underpins many statistical learning techniques. Real-world returns are heteroskedastic, exhibit regime shifts, and often have heavy-tailed distributions [Cont, 2001]. GARCH-type models [Engle, 1982, Bollerslev, 1986] can capture some volatility clustering, but they still depend on pre-specified distributions and lack reliable coverage guarantees for interval forecasts.

In recent years, conformal prediction has gained traction as a powerful distribution-free framework for quantifying uncertainty. Classical conformal methods provide finite-sample coverage guarantees without assuming a particular data distribution [Vovk et al., 2005]. However, these guarantees rest on exchangeability, a condition often violated by time series with temporal dependencies. Several works extend conformal methods to sequential or temporally dependent settings [Xu and Xie, 2021, Stankeviciute et al., 2021, Gibbs and Candès, 2021], but a robust and practical solution for financial markets remains an open challenge.

This paper closes that gap. We introduce **Temporal Conformal Prediction (TCP)**, a real-time, adaptive framework for constructing well-calibrated prediction intervals for financial time series. TCP combines a modern machine-learning quantile forecaster with an online conformal calibration layer governed by a modified Robbins–Monro scheme. Crucially, this architecture bridges statistical inference and machine learning, combining the theoretical rigor of conformal methods with the flexibility of a data-driven approach that can adapt to non-stationarity, volatility clustering, and abrupt market shifts.

We benchmark TCP across three major asset classes, **equities (S&P 500)**, **cryptocurrency (Bitcoin)**, and **commodities (Gold)**, against established models like GARCH, Historical Simulation, and standard Quantile Regression (QR). Our results highlight a critical flaw in static ML approaches: while QR produces sharp intervals, it is poorly calibrated and systematically misses the 95% target. By contrast, TCP demonstrates superior adaptive capabilities, adjusting its intervals in response to market volatility to better align with the desired coverage rate. This adaptive property, which we visualize during the March 2020 crash, makes TCP a more reliable and principled framework for real-world risk management. A comprehensive sensitivity analysis further underscores the robustness of our framework to key hyperparameters.

We organize the paper as follows. Section 2 surveys related work. Section 3 establishes our mathematical notation. Section 4 lays out the TCP theory. Section 5 details our empirical setup, including model architectures and the evaluation framework. Section 6 presents our main findings, including benchmark comparisons, visualizations, and hyperparameter sensitivity analysis. Finally, Section 7 offers practical takeaways and future directions.

## 2. RELATED WORK

Before detailing our proposed TCP framework, we situate our work within the existing literature. We review three areas that inform our approach: traditional financial risk models, the evolution of time-series forecasting with machine learning, and the theoretical foundations of conformal prediction.

**Traditional Financial Risk Models.** Quantitative risk management traces its roots to portfolio theory [Markowitz, 1952] and was formalized around the VaR concept with J.P.

Morgan’s RiskMetrics [J.P. Morgan/Reuters, 1996]. In practice, three VaR paradigms have dominated: *parametric* approaches (often assuming conditional normality), *non-parametric* Historical Simulation, and *Monte Carlo* methods [Jorion, 2007, Dowd, 1998, Glasserman, 2004]. Beyond VaR, CVaR provided a coherent alternative for tail-risk control [Rockafellar and Uryasev, 2000]. However, many traditional approaches underperform in crisis backtests [Kupiec, 1995, Christoffersen, 1998], highlighting a blind spot when tail events dominate.

**Advanced Time-Series and Machine-Learning Models.** To better capture time-varying variance and volatility clustering, the GARCH family became foundational [Engle, 1982, Bollerslev, 1986]; asymmetric variants such as *EGARCH* and *GJR-GARCH* address leverage and sign effects [Nelson, 1991, Glosten et al., 1993]. For heavy-tailed markets, extreme value theory (EVT) offers principled tail modeling [III, 1975, McNeil and Frey, 2000], and VaR under heavy tails raises specific concerns [Danielsson and de Vries, 2000]. On the machine-learning side, quantile regression directly targets conditional quantiles [Koenker and Bassett, 1978], with ensemble and neural variants such as quantile regression forests [Meinshausen, 2006] and quantile networks [Taylor, 2000]; deep LSTMs capture complex temporal dependencies [Fischer and Krauss, 2018]. We also emphasize the computational efficiency of gradient-boosted trees via LightGBM for quantile forecasting [Ke et al., 2017].

**Conformal Prediction Theory.** Conformal prediction provides distribution-free, finite-sample prediction sets under exchangeability [Vovk et al., 2005]. Recent advances relax these assumptions for sequential or non-stationary settings through adaptive calibration and time-series-aware procedures [Gibbs and Candès, 2021, Xu and Xie, 2021, Stankeviciute et al., 2021]. Our work builds on these foundations with a practical adaptive conformal framework tailored to financial risk forecasting, combining local split-conformal calibration with an online Robbins–Monro offset for temporal adaptation.

### 3. NOTATION

Having reviewed the relevant literature, we now establish the mathematical notation that will be used throughout the remainder of the paper. A clear notational framework is essential for formally developing our proposed method in the subsequent sections.

We denote the price of a financial asset at time  $t$  as  $P_t$ , and its corresponding daily log-return as  $r_t$ . The primary objective is to construct a  $(1 - \alpha)$  prediction interval, denoted by  $[\ell_{t+1}, u_{t+1}]$ , for the next return  $r_{t+1}$ , where  $\alpha \in (0, 1)$  is the specified miscoverage rate. The feature space for our models includes lagged returns and realized volatility  $\sigma_t$ .

**Learning and Prediction:** For a general learning problem with  $n$  observations, we consider feature-label pairs as  $(X_i, Y_i)$  and a generic point prediction model as  $\hat{f}(\cdot)$ . Our time series evaluation runs for  $T$  total time steps. We use  $\mathcal{F}_t$  to represent the filtration (information set) available up to time  $t$ . The true, unknown  $\tau$ -quantile of the return distribution is  $q_\tau$ . Our quantile regression model,  $\mathcal{F}_\tau$ , produces a data-driven estimate of this quantile, denoted  $\hat{q}_\tau$ .

**Conformal Prediction (two-sided, split).** At each time  $t$  we use a rolling window of size  $w$  split into a training slice  $\mathcal{T}_t$  and a calibration slice  $\mathcal{C}_t$  with  $|\mathcal{T}_t| + |\mathcal{C}_t| = w$ . Quantile forecasters  $\hat{q}_{\alpha/2}$  and  $\hat{q}_{1-\alpha/2}$  are fit on  $\mathcal{T}_t$  only (no leakage). Two-sided nonconformity scores on the calibration slice are

$$s_i = \max\{\hat{q}_{\alpha/2}(X_i) - r_i, r_i - \hat{q}_{1-\alpha/2}(X_i), 0\}, \quad i \in \mathcal{C}_t.$$

Let  $m = |\mathcal{C}_t|$  and  $s_{(1)} \leq \dots \leq s_{(m)}$  be the order statistics. We set the conformal threshold  $C_t = s_{(k)}$  with  $k = \lceil (m + 1)(1 - \alpha) \rceil$ , and the next-step interval  $[\ell_{t+1}, u_{t+1}] = [\hat{q}_{\alpha/2}(X_{t+1}) -$

$C_t$ ,  $\widehat{q}_{1-\alpha/2}(X_{t+1}) + C_t$ ]. For comparability, the QR baseline is evaluated in the same walk-forward fashion using only the training slice  $|\mathcal{T}_t|=w_{\text{tr}}$  (no calibration slice), i.e., it is rolling and out-of-sample.

**Adaptive Calibration:** The online adaptive calibration is driven by the coverage error at time  $t$ , defined as  $e_t = \mathbb{1}(r_t \notin [\ell_t, u_t]) - \alpha$ . The threshold is updated using a learning rate  $\gamma_t$ , which is itself controlled by hyperparameters  $\gamma_0, \lambda$ , and  $\beta$ .

**Benchmark Models:** For the benchmark models, we denote the conditional variance from the GARCH model as  $\hat{\sigma}_t^2$ , which is governed by parameters  $\omega, \alpha_{\text{GARCH}}$ , and  $\beta_{\text{GARCH}}$ . For Historical Simulation, we use  $\bar{r}$  to represent the mean return over a rolling window.

**Mathematical Operators:** Finally, we use standard mathematical operators, including  $\Pr(\cdot)$  for probability,  $\mathbb{E}[\cdot]$  for expectation,  $\mathbf{1}(\cdot)$  for the indicator function,  $\text{sign}(\cdot)$  for the sign function, and  $\lfloor \cdot \rfloor$  for the floor function.

**Variants used (terminology).** We consider two closely related procedures. **TCP** denotes split-conformal prediction on a rolling window: the window  $\mathcal{W}_t$  of size  $w$  is split into a training slice  $\mathcal{T}_t$  (size  $w_{\text{tr}}$ ) and a calibration slice  $\mathcal{C}_t$  (size  $w_{\text{cal}}$ ),  $w_{\text{tr}} + w_{\text{cal}} = w$ . Quantile forecasters  $\widehat{q}_{\alpha/2}, \widehat{q}_{1-\alpha/2}$  are fit on  $\mathcal{T}_t$  only and the two-sided split-conformal threshold  $C_t$  is computed from  $\mathcal{C}_t$ , yielding  $[\ell_{t+1}, u_{t+1}] = [\widehat{q}_{\alpha/2}(X_{t+1}) - C_t, \widehat{q}_{1-\alpha/2}(X_{t+1}) + C_t]$ . **TCP-RM** augments TCP with an online *Robbins-Monro* (RM) offset  $C_t^{\text{RM}}$  updated by  $C_{t+1}^{\text{RM}} = C_t^{\text{RM}} + \gamma_t \{\mathbf{1}(r_t \notin [\ell_t, u_t]) - \alpha\}$ , with  $\gamma_t = \gamma_0(1 + \lambda t)^{-\beta}$ . The effective threshold is  $C_t^{\text{eff}} = C_t + C_t^{\text{RM}}$  and the interval becomes  $[\widehat{q}_{\alpha/2}(X_{t+1}) - C_t^{\text{eff}}, \widehat{q}_{1-\alpha/2}(X_{t+1}) + C_t^{\text{eff}}]$ . For comparability, the QR baseline is evaluated in the same walk-forward fashion using only the training slice ( $|\mathcal{T}_t| = w_{\text{tr}}$ ) and *no* calibration slice (rolling, out-of-sample).

## 4. MATHEMATICAL BACKGROUND

This section lays the theoretical groundwork for our proposed method. We begin by formally defining the problem of prediction interval forecasting, then review the principles of classical conformal prediction and its limitations, and finally develop the core mathematical components of our Temporal Conformal Prediction (TCP) framework and its adaptive calibration mechanism.

### 4.1 Problem Formulation

We begin by framing the central task of this paper. We consider a univariate financial time series of daily log-returns  $\{r_1, r_2, \dots, r_t\}$ , where  $r_t = \log(P_t/P_{t-1})$  and  $P_t$  is the asset price at time  $t$ . Our objective is to construct a prediction interval  $[\ell_{t+1}, u_{t+1}]$  for the next return  $r_{t+1}$  that satisfies the nominal coverage property  $\Pr(r_{t+1} \in [\ell_{t+1}, u_{t+1}]) \approx 1 - \alpha$  for a given miscoverage level  $\alpha \in (0, 1)$ . Traditional methods often fail to achieve this in the presence of non-stationarity, motivating our distribution-free approach.

### 4.2 Classical Conformal Prediction

To motivate our approach, we first briefly review the classical conformal prediction framework, which provides strong guarantees but relies on an assumption that is often violated in our target domain.

Given a set of i.i.d. observations  $\{(X_i, Y_i)\}_{i=1}^n$  from an unknown distribution, conformal prediction provides a framework for generating prediction sets with finite-sample coverage guar-

antees. This is achieved through a non-conformity score.

**Definition 4.1 (Non-Conformity Score)** *A mapping  $A((X_i, Y_i)) \mapsto \alpha_i \in \mathbb{R}$  that quantifies how poorly a data point  $(X_i, Y_i)$  conforms to a given model or dataset. A higher score implies a poorer fit.*

For a new test point  $X_{n+1}$ , the prediction set  $\Gamma_{1-\alpha}(X_{n+1})$  is formed by all possible values  $y$  whose non-conformity score  $A(X_{n+1}, y)$  is less than or equal to the  $(1 - \alpha)$ -quantile of the scores from the training set. Formally, if we define the empirical p-value for a candidate value  $y$  as  $p(y) = \frac{1}{n+1} \sum_{i=1}^{n+1} \mathbf{1}(\alpha_i \geq A(X_{n+1}, y))$ , the prediction set is:

$$\Gamma_{1-\alpha}(X_{n+1}) = \{y : p(y) > \alpha\}.$$

**Theorem 4.1 (Finite-Sample Validity)** *If the sequence of pairs  $\{(X_i, Y_i)\}_{i=1}^{n+1}$  is exchangeable, then the conformal prediction set  $\Gamma_{1-\alpha}$  satisfies:*

$$\Pr(Y_{n+1} \in \Gamma_{1-\alpha}(X_{n+1})) \geq 1 - \alpha.$$

A common choice for the non-conformity score is the absolute residual,  $\alpha_i = |Y_i - \hat{f}(X_i)|$ , where  $\hat{f}$  is a point prediction model.

A full proof is provided in Appendix A.

### 4.3 Temporal Conformal Prediction (TCP)

The exchangeability assumption required by classical conformal prediction is too restrictive for financial time series. Here, we build upon its principles to develop our TCP method, which relaxes this assumption to hold only within a local time window. Our proposed TCP method, outlined in Algorithm 1, leverages this principle.

**Algorithm 1** Temporal Conformal Prediction (TCP) at time  $t$  (split-conformal, two-sided)

**Require:** Returns  $\{r_1, \dots, r_t\}$ ; features  $\{X_1, \dots, X_t\}$ ; window  $w$  with  $w_{\text{tr}} + w_{\text{cal}} = w$ ; misscoverage  $\alpha \in (0, 1)$

1: **Define slices:**  $\mathcal{W}_t = \{t-w+1, \dots, t\}$ ;  $\mathcal{T}_t = \{t-w+1, \dots, t-w_{\text{cal}}\}$ ;  $\mathcal{C}_t = \{t-w_{\text{cal}}+1, \dots, t\}$

2: **Fit forecasters on  $\mathcal{T}_t$ :** train  $\hat{q}_{\alpha/2}, \hat{q}_{1-\alpha/2}$  on  $\{(X_i, r_i) : i \in \mathcal{T}_t\}$

3: **Compute two-sided nonconformity on  $\mathcal{C}_t$ :**

4: **for each  $i \in \mathcal{C}_t$  do**

5:  $s_i \leftarrow \max\{\hat{q}_{\alpha/2}(X_i) - r_i, r_i - \hat{q}_{1-\alpha/2}(X_i), 0\}$

6:  $m \leftarrow |\mathcal{C}_t|$ ; sort  $s_{(1)} \leq \dots \leq s_{(m)}$

7: **Conformal threshold:**  $k \leftarrow \lceil (m+1)(1-\alpha) \rceil$ ;  $C_t \leftarrow s_{(k)}$

8: **Form next-step interval:**

9:  $\ell_{t+1} \leftarrow \hat{q}_{\alpha/2}(X_{t+1}) - C_t$ ;  $u_{t+1} \leftarrow \hat{q}_{1-\alpha/2}(X_{t+1}) + C_t$

**Ensure:** Prediction interval  $[\ell_{t+1}, u_{t+1}]$

### 4.4 Adaptive Calibration (TCP vs. TCP-RM)

We consider two variants. **TCP** is split-conformal only: at each time  $t$ , the window  $\mathcal{W}_t$  of size  $w$  is split into a training slice  $\mathcal{T}_t$  and a calibration slice  $\mathcal{C}_t$  with  $|\mathcal{T}_t| + |\mathcal{C}_t| = w$ . Quantile forecasters

$\widehat{q}_{\alpha/2}, \widehat{q}_{1-\alpha/2}$  are fit on  $\mathcal{T}_t$  and the two-sided nonconformity scores on  $\mathcal{C}_t$  yield the split-conformal threshold  $C_t = s_{(k)}$ ,  $k = \lceil (|\mathcal{C}_t| + 1)(1 - \alpha) \rceil$ . **TCP-RM** augments TCP with a single online offset  $C_t^{\text{RM}}$  updated by Robbins–Monro:

$$C_{t+1}^{\text{RM}} = C_t^{\text{RM}} + \gamma_t \left( \mathbf{1}\{r_t \notin [\ell_t, u_t]\} - \alpha \right), \quad (1)$$

$$\gamma_t = \frac{\gamma_0}{(1 + \lambda t)^\beta}, \quad \beta \in (1/2, 1]. \quad (2)$$

The effective threshold is  $C_t^{\text{eff}} = C_t + C_t^{\text{RM}}$ , giving  $[\ell_{t+1}, u_{t+1}] = [\widehat{q}_{\alpha/2}(X_{t+1}) - C_t^{\text{eff}}, \widehat{q}_{1-\alpha/2}(X_{t+1}) + C_t^{\text{eff}}]$ . No manual decay or heuristic shrinkage is used.

**Assumptions.** (A1) (*Bounded scores*)  $\{s_i\}$  are a.s. bounded. (A2) (*Local mixing*) The process is  $\beta$ -mixing so that  $e_t - \mathbb{E}[e_t \mid \mathcal{F}_{t-1}]$  is a martingale-difference with bounded variance. (A3) (*Monotone coverage in  $C$* )  $g(C) = \Pr(r_t \in [\ell_t, u_t] \mid C)$  is continuous and strictly increasing near the unique  $C^*$  with  $g(C^*) = 1 - \alpha$ . (A4) (*Stepsizes*)  $\gamma_t > 0$ ,  $\sum_t \gamma_t = \infty$ ,  $\sum_t \gamma_t^2 < \infty$ .

Under (A1)–(A4), TCP provides local finite-sample validity on  $\mathcal{C}_t$ ; TCP-RM adds asymptotic calibration in time via (1).

## 4.5 Proof of Asymptotic Calibration

**Theorem 4.2** *Under the Robbins–Monro update (1) and (A1)–(A4),  $\frac{1}{T} \sum_{t=1}^T \mathbf{1}\{r_t \in [\ell_t, u_t]\} \rightarrow 1 - \alpha$  a.s., and  $C_t \rightarrow C^*$  a.s.*

Full proof is given in Appendix A.

**Remark 4.1 (Practical stability)** *To enforce (A1) and keep the iterates bounded, we only enforce nonnegativity of the effective threshold by projecting the RM offset:*

$$C_{t+1}^{\text{RM}} \leftarrow \max \left\{ C_t^{\text{RM}} + \gamma_t (\mathbf{1}\{r_t \notin [\ell_t, u_t]\} - \alpha), -C_t \right\},$$

so that  $C_{t+1}^{\text{eff}} = C_t + C_{t+1}^{\text{RM}} \geq 0$ . An additional upper cap  $S_t$  (e.g., a high empirical quantile of the calibration scores  $s_i$ ) can be included, but we did not use it in our experiments. This projection is standard in stochastic approximation and does not change the prediction rule.

## 5. METHODOLOGY

With the theoretical foundations of TCP established in the previous section, we now turn to our empirical study. This section details the methodology used to evaluate TCP’s performance, including the data and features, the specific model implementations, and the evaluation framework.

### 5.1 Data and Feature Construction

The foundation of any forecasting model is the data it learns from. We begin by describing the financial assets used in our analysis and the construction of the feature set designed to capture relevant market dynamics.

We analyze daily log-returns,  $r_t = \log(P_t/P_{t-1})$ , for three distinct asset classes: **Equities** (S&P 500), **Cryptocurrencies** (Bitcoin), and **Commodities** (Gold), using data from November 2017 to May 2025. For each asset, we construct a feature set for our models based on recent historical data. The features include:

- **Lagged Returns:**  $\{r_{t-k}\}_{k=1}^5$  to capture short-term momentum and autoregressive effects.
- **Rolling Volatility:**  $\sigma_t = \sqrt{\frac{1}{20-1} \sum_{k=1}^{20} (r_{t-k} - \bar{r}_{t,20})^2}$  (rolling sample std, ddof=1) where  $\bar{r}_{t,20} = \frac{1}{20} \sum_{k=1}^{20} r_{t-k}$ .
- **Nonlinear Transformations:** The squared prior return,  $r_{t-1}^2$ , and its sign,  $\text{sign}(r_{t-1})$ , to account for non-linear dependencies and leverage effects.

In implementation we use the rolling sample standard deviation via `pandas (.rolling(20).std, ddof= 1)`.

## 5.2 Forecasting Models

To fairly assess the contribution of our proposed method, we benchmark it against several established alternatives. Here, we describe the implementation of TCP and the three competing models: Quantile Regression, GARCH, and Historical Simulation.

### 5.2.1 Temporal Conformal Prediction (TCP)

Our proposed model first estimates the conditional quantiles,  $\hat{q}_\tau(t)$ , using a gradient-boosted tree model,  $\mathcal{F}_\tau$ , trained on the feature set described above. The prediction interval is formed from the forecaster’s two quantiles and the split-conformal threshold  $C_t$  computed on a disjoint calibration slice (Alg. 1). In the TCP-RM variant,  $C_t$  is further updated online via (1). This threshold is updated at each time step based on the observed coverage error, as detailed in Section 4. The entire process is performed sequentially on a rolling basis with a window of  $w = 252$  days.

### 5.2.2 Benchmark Models

1. **Quantile Regression (QR):** Same gradient-boosted quantile forecaster as TCP, evaluated sequentially in a *rolling, out-of-sample* manner on a trailing window of  $w_{\text{tr}}=192$  observations (no conformal calibration).
2. **Fixed-parameter GARCH(1,1) (EWMA):** Conditional variance updated recursively

$$\sigma_t^2 = \omega + \alpha r_{t-1}^2 + \beta \sigma_{t-1}^2, \quad (\omega, \alpha, \beta) = (10^{-6}, 0.05, 0.9),$$

with coefficients held fixed and updated sequentially using only past data (no rolling re-estimation). One-step-ahead  $(1 - \alpha)$  intervals assume conditional normality with zero mean, i.e.,  $[-z_{1-\alpha/2}\sigma_t, z_{1-\alpha/2}\sigma_t]$ .

3. **Historical Simulation (Hist):** Non-parametric empirical  $(\alpha/2, 1 - \alpha/2)$  quantiles from a rolling 252-day window.

## 5.3 Evaluation Framework

To provide a rigorous comparison, we must define clear success criteria. This subsection outlines the key performance metrics, empirical coverage and interval sharpness, that we use to evaluate and contrast the models. We use two primary metrics:

- **Empirical Coverage:** The proportion of out-of-sample observations that fall within their respective prediction intervals,  $\frac{1}{T} \sum_{t=1}^T \mathbf{1}\{r_t \in [\ell_t, u_t]\}$ . The primary goal is to match the nominal coverage rate of  $1 - \alpha = 95\%$ .
- **Average Interval Width (Sharpness):** The average width of the prediction intervals,  $\frac{1}{T} \sum_{t=1}^T (u_t - \ell_t)$ . Sharper (narrower) intervals are preferred, provided that the target coverage is met.

Our analysis focuses on the trade-off between these two metrics, as a model is only useful if it is both well-calibrated (correct coverage) and sharp (informative).

## 6. RESULTS AND DISCUSSION

We now assess **Temporal Conformal Prediction (TCP)** and our main contribution **TCP-RM** (TCP with a Robbins–Monro online calibration layer) against strong baselines (QR, GARCH, Historical Simulation) on three asset classes: *S&P 500*, *BTC-USD*, and *Gold*. The goal is to test whether the online calibration delivers near-nominal coverage under distribution shift while preserving sharpness.

Evaluation centers on two criteria: (i) *empirical coverage* versus the nominal target  $1 - \alpha = 0.95$ , and (ii) *average interval width* as a measure of sharpness. Table 1 summarizes full-sample performance; Figure 1 visualizes behavior during the COVID-19 crash. We also report a hyperparameter sensitivity study (window size  $w$ , stepsize  $\gamma_0$ ) to assess robustness of TCP-RM.

Table 1: Model Performance Across Assets (Target Coverage: 95%)

Asset	Model	Empirical Coverage	Avg. Interval Width	Predictions
SP500	TCP	0.9441	3.5975	1449
	TCP-RM	0.9469	3.6068	1449
	QR	0.8628	2.686	1509
	GARCH	0.8269	3.0505	1670
	Hist	0.9312	5.0575	1468
BTC-USD	TCP	0.9586	11.2346	1449
	TCP-RM	0.9593	11.2374	1449
	QR	0.8960	9.8446	1509
	GARCH	0.8533	11.3908	1670
	Hist	0.9441	18.0576	1468
Gold	TCP	0.9427	2.6630	1449
	TCP-RM	0.9448	2.6696	1449
	QR	0.8761	2.2394	1509
	GARCH	0.8365	2.6185	1670
	Hist	0.9326	4.0238	1468

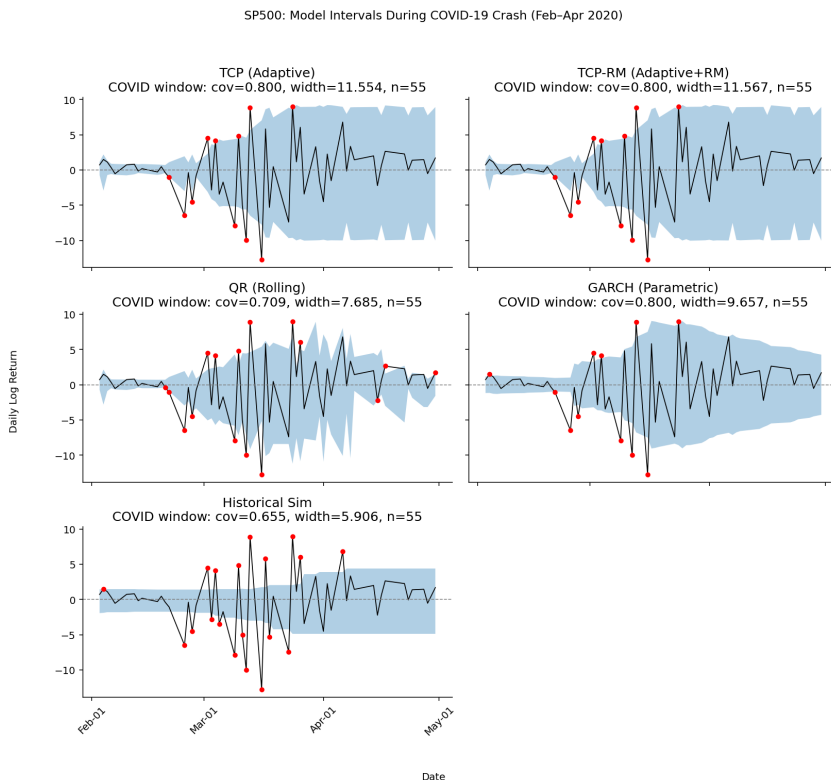


Figure 1: A comparison of 95% prediction intervals from **five** models (TCP, TCP-RM, QR, GARCH, Hist) for S&P 500 daily returns during the COVID-19 market crash (Feb–Apr 2020). Shaded bands show the interval; the **red dots** mark days where the realized return falls outside the 95% interval (miscoverage). TCP/TCP-RM bands widen rapidly into the March spike and contract in April, illustrating adaptiveness. Analogous crisis-window panels for BTC-USD and Gold appear in Appendix B.

## 6.1 Main Findings: Adaptiveness and Calibration

Three findings emerge clearly from Table 1 and the crisis-window visualization (Fig. 1):

1. **(i) Calibration vs. sharpness trade-off.** The rolling ML baseline (QR) produces the **narrowest** intervals across all assets but is **materially under-calibrated** relative to the 95% target: SP500 86.3%, BTC 89.6%, Gold 87.6%. This under-coverage is the price for sharpness (e.g., SP500 average width 2.686 versus TCP’s 3.598). In other words, rolling QR concentrates mass too aggressively in volatile regimes.
2. **(ii) TCP/TCP-RM achieve near-nominal coverage with substantially tighter bands than Historical Simulation.** TCP coverage is close to the target on all assets (SP500 94.4%, BTC 95.9%, Gold 94.3%), while keeping intervals **30–38% narrower than Historical Simulation**: SP500: 3.598 vs 5.058 (–28.9%); BTC: 11.235 vs 18.058 (–37.8%); Gold: 2.663 vs 4.024 (–33.8%). Thus, TCP delivers a better calibration–sharpness balance than Hist, which attains decent coverage but with overly conservative widths.
3. **(iii) Robbins–Monro improves calibration at essentially no cost in width.** TCP-RM yields a **small positive lift in coverage** relative to TCP with **negligible** width

change on all assets (e.g., SP500: +0.28 percentage points coverage, +0.009 width). This supports the utility of the online offset for fine-tuning calibration without sacrificing sharpness.

GARCH under-covers consistently ( $\approx 0.83$ – $0.85$ ) while not being as sharp as QR, suggesting its conditional-Gaussian volatility path is too slow to adapt to return asymmetries and tail thickness during stress.

**Crisis-window behavior.** Figure 1 (SP500, Feb–Apr 2020) shows how each method behaves during the shock. The *red dots* mark days where the realized return falls *outside* the reported 95% prediction interval (i.e., miscoverage events). TCP bands **widen abruptly in early March**, remain elevated through the peak volatility in mid–late March, and **begin to contract** in April as conditions stabilize. TCP and TCP-RM deliver similar behavior and, in this short 55-day window, both achieve coverage of  $\approx 0.80$  with average widths  $\approx 11.55$ – $11.57$ . Rolling QR widens only modestly, keeps **much tighter** bands (width = 7.69), and shows **the most red dots around the extremes**, consistent with its lower window coverage (0.709). GARCH ramps up more smoothly, reflecting its volatility recursion, and lands at the same window coverage as TCP (0.800) with narrower bands (width = 9.66). Historical Simulation reacts more slowly and is the most under-covered here (0.655), despite having the narrowest bands in this window (width = 5.91); this lag is expected from its long empirical lookback. Overall, the crisis snapshot illustrates a general pattern under abrupt regime change: all methods temporarily under-cover, but TCP/TCP-RM **adapt fastest by inflating bands right when volatility jumps**, while QR remains sharp at the cost of additional misses. This visual evidence complements the full out-of-sample results in Table 1, where TCP/TCP-RM recover to near-nominal calibration over the full evaluation horizon. Analogous crisis-window panels for BTC-USD and Gold are reported in the Appendix B.

*Implementation note (comparability).* All learning-based methods use the same feature set. TCP/TCP-RM are evaluated out-of-sample with a rolling window of 252 points split into 192 training and 60 calibration points. Rolling QR is also evaluated out-of-sample using a **192-point trailing training window**. The slight differences in the “Predictions” counts (e.g., 1509 for QR vs. 1449 for TCP/TCP-RM) reflect different warm-up requirements (QR does not reserve a calibration slice). Aligning the evaluation horizon to the longest warm-up yields qualitatively identical conclusions: QR is sharp but under-calibrated; TCP/TCP-RM are near-nominal and materially sharper than Historical Simulation.

## 6.2 Hyperparameter Sensitivity (SP500, TCP-RM)

We stress-test the adaptive layer by varying the rolling window  $w$  and the initial step size  $\gamma_0$  for **TCP-RM** (Table 2). For comparability we fix the calibration slice at  $|\mathcal{C}| = 40$  and sweep  $w \in \{100, 252, 500\}$  and  $\gamma_0 \in \{0.005, 0.01, 0.05\}$  on **SP500**. Results for BTC-USD and Gold exhibit the same pattern and are reported in Appendix D.

*What we learn.* (i) Increasing  $w$  consistently sharpens intervals: widths fall from  $\approx 4.52$  ( $w=100$ ) to 3.26–3.40 ( $w=500$ ), while coverage stays at or above the target band. (ii) At a fixed  $w$ , larger  $\gamma_0$  nudges coverage upward with a small width trade-off; e.g., at  $w=252$ ,  $\gamma_0=0.050$  lifts coverage from 0.9469 to 0.9524 (+0.55pp) with a  $\sim 0.03$  increase in width; at  $w=500$ , very large  $\gamma_0$  overshoots the target (0.9759).

*Takeaway.* TCP-RM is robust to reasonable choices of  $(w, \gamma_0)$ . For the main experiments, we retain  $w=252$  and  $\gamma_0=0.01$ , which stay near the nominal level while keeping intervals tight; if one prefers even sharper intervals,  $w=500$  with  $\gamma_0 \in [0.005, 0.01]$  is a good choice without

Table 2: TCP-RM sensitivity on S&P 500 with  $|\mathcal{C}| = 40$  (target 95%).

Hyperparameters		Performance	
Window Size ( $w$ )	$\gamma_0$	Coverage	Interval Width
100	0.005	0.9557	4.5188
100	0.010	0.9557	4.5202
100	0.050	0.9550	4.5315
252	0.005	0.9469	3.4605
252	0.010	0.9469	3.4673
252	0.050	0.9524	3.4878
500	0.005	0.9559	3.2627
500	0.010	0.9659	3.2815
500	0.050	0.9759	3.3970

material over-coverage.

We also perform sensitivity analysis on TCP. The results are given in Appendix E.

### 6.3 Visualization for TCP vs. TCP-RM on S&P 500 (95% intervals)

In this section, we present the TCP vs TCP-RM trace plot for S&P 500.

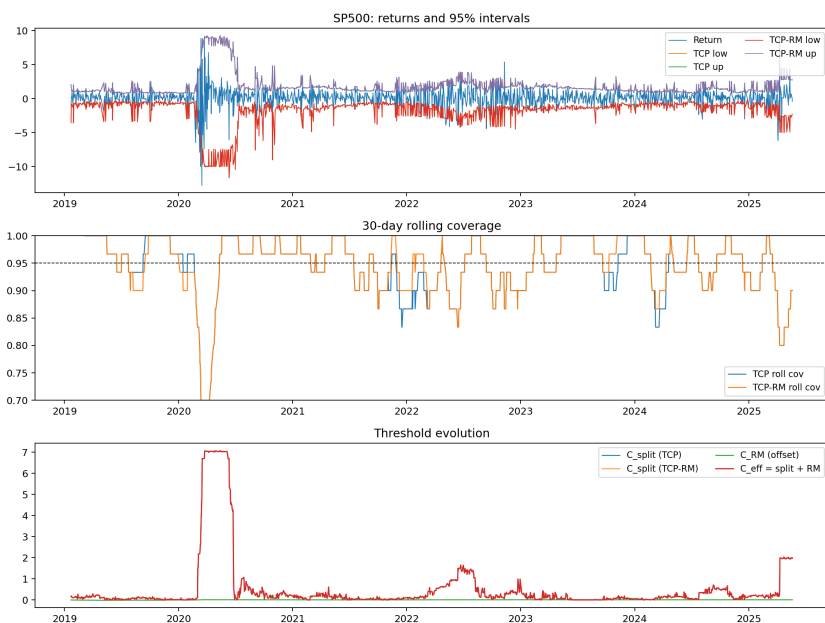


Figure 2: **TCP vs. TCP-RM on S&P 500 (95% intervals)**. *Top*: daily returns with two-sided prediction bands for TCP (blue) and TCP-RM (purple). *Middle*: 30-day rolling empirical coverage; the dashed line marks the 95% target. *Bottom*: evolution of conformal thresholds: split-conformal level  $C_{\text{split}}$ , online Robbins–Monro offset  $C_{\text{RM}}$ , and the effective total  $C_{\text{eff}} = C_{\text{split}} + C_{\text{RM}}$ . During the COVID-19 crash the bands widen sharply, the rolling coverage briefly departs from the 95% target and then re-enters the band, and  $C_{\text{eff}}$  spikes before decaying as conditions stabilize.

In Fig. 2, TCP and TCP-RM behave similarly in tranquil periods, but during stress the effective threshold  $C_{\text{eff}}$  (bottom panel) rises quickly, producing wider bands (top) and steering the 30-day rolling coverage back toward the 95% target (middle). The Robbins–Monro offset  $C_{\text{RM}}$  remains near zero except around regime shifts, where it provides the extra adjustment that closes the gap to target coverage. This visual evidence complements Table 1: on S&P 500, TCP-RM attains  $\approx 95\%$  coverage with only a marginal width increase relative to TCP

## 7. CONCLUSION AND FUTURE WORK

This paper introduced **Temporal Conformal Prediction (TCP)**, a simple and effective framework for calibrated prediction intervals in nonstationary time series. TCP combines a rolling, exchangeability-aware split–conformal layer with a modern quantile forecaster, and the **TCP–RM** variant adds a single Robbins–Monro offset that adjusts the conformal threshold online using observed coverage errors.

Across three asset classes, TCP/TCP–RM deliver a strong calibration–sharpness balance: coverage is close to the 95% target while intervals are materially narrower than Historical Simulation. In contrast, the *rolling* QR baseline attains the narrowest bands but *undershoots* the target coverage, especially in turbulent regimes. Crisis-window visualizations around the COVID-19 crash illustrate TCP’s intended adaptiveness: intervals widen rapidly as volatility spikes and contract as conditions stabilize, with red dots indicating miscoverage events. A targeted sensitivity analysis shows robustness to reasonable choices of rolling window and Robbins–Monro step size, and suggests default settings that are stable in practice.

**Limitations.** Like any sequential method, TCP can temporarily under-cover during abrupt regime shifts before its calibration catches up. Performance also inherits the quality of the base quantile forecaster and the choice of windowing; extremely heavy tails or structural breaks can stress any fixed feature set. Finally, while TCP–RM improves calibration at negligible width cost on average, very aggressive step sizes can overcorrect.

**Practical implications.** By providing distribution-free intervals that adapt in time, TCP aligns naturally with backtesting and governance needs in risk management (coverage targets, exception tracking, and scenario robustness). The framework is lightweight (single threshold) and model-agnostic (plugs into any quantile forecaster), making deployment straightforward in production pipelines.

### 7.1 Future Work

Several extensions follow naturally:

1. **Multivariate and portfolio TCP.** Generalize to joint/conditional quantiles for baskets of assets; couple TCP with copula or factor models to control portfolio-level coverage.
2. **Conditional and localized coverage.** Target coverage conditional on covariates (e.g., volatility state) and explore adaptive nonconformity scores that emphasize tail risk or signed errors.
3. **Richer forecasters and features.** Swap the base learner for neural quantile models or boosted variants with realized-volatility inputs (intraday RV), order-flow, or macro features; assess benefits for sharpness at fixed coverage.
4. **Change–point aware adaptation.** Trigger temporary step–size boosts or threshold projections when a regime break is detected to shorten the transient under/over-shoot in cover-

age.

5. **Heavy-tail robustness.** Investigate EVT-inspired nonconformity scores or asymmetric penalties to better stabilize performance under extreme shocks.
6. **Decision integration.** Map TCP intervals to VaR/ES, margin, and capital rules; evaluate utility/capital efficiency vs. conservative baselines in realistic backtests.
7. **Beyond finance.** TCP’s adaptiveness is broadly applicable wherever nonstationarity and calibrated uncertainty matter:
  - *Biostatistics/medicine:* ICU vitals monitoring and glucose-range forecasting with patient-specific adaptation; adaptive dosing intervals under drift.
  - *Epidemiology:* Calibrated intervals for nowcasts/forecasts of incidence and  $R_t$  that widen under reporting delays or testing-policy shifts, plus adaptive risk bands for hospitalization/ICU load as transmission regimes change.
  - *Genetics/Genomics:* Uncertainty bands for polygenic risk scores and eQTL effect sizes that remain calibrated under population/covariate shift; interval forecasts for gene expression (bulk or single-cell) with batch effects and sequencing-depth drift; calibrated pathogenicity scores for rare variants.
  - *Sports analytics:* Game-state-aware intervals for win probability, expected goals/points, and player performance that adapt to tempo and lineup changes; injury-risk ranges for load management with rapid recalibration after shocks (e.g., in-game injuries or schedule congestion).
  - *Renewable energy:* Wind/solar generation intervals that expand/contract with weather regimes to aid grid balancing.
  - *Operations/marketing:* Demand and lead-time intervals for inventory control; calibrated lift ranges in marketing-mix models under campaign drift.
  - *Transportation and climate:* Travel-time intervals under traffic regime shifts; local hazard/risk bands for extreme weather.

In sum, TCP offers a compact, distribution-free, and *adaptive* route to calibrated uncertainty quantification in the presence of temporal drift. Its empirical performance, visual adaptiveness in crisis windows, and robustness to sensible hyperparameters suggest it is a practical default for risk forecasting and a promising building block for broader sequential decision systems.

## 8. DATA AND CODE AVAILABILITY

The financial returns dataset and all code used in this paper are publicly available at: <https://github.com/agnivibes/temporal-conformal-prediction-tcp>.

## References

- Tim Bollerslev. Generalized autoregressive conditional heteroskedasticity. *Journal of Econometrics*, 31(3):307–327, 1986.
- Markus K. Brunnermeier. Deciphering the liquidity and credit crunch 2007–2008. *Journal of Economic Perspectives*, 23(1):77–100, 2009.

- Peter F. Christoffersen. Evaluating interval forecasts. *International Economic Review*, 39(4): 841–862, 1998.
- Rama Cont. Empirical properties of asset returns: Stylized facts and statistical issues. *Quantitative Finance*, 1(2):223–236, 2001.
- Jon Danielsson and Casper G. de Vries. Value-at-risk and extreme returns. *Annals of Economics and Statistics*, 60:239–270, 2000.
- Kevin Dowd. *Beyond Value-at-Risk: The New Science of Risk Management*. John Wiley & Sons, Chichester, UK, 1998.
- Robert F. Engle. Autoregressive conditional heteroskedasticity with estimates of the variance of united kingdom inflation. *Econometrica*, 50(4):987–1007, 1982.
- Thomas Fischer and Christopher Krauss. Deep learning with long short-term memory networks for financial market predictions. *European Journal of Operational Research*, 270(2):654–669, 2018.
- Isaac Gibbs and Emmanuel Candès. Adaptive conformal inference under distribution shift. In *Advances in Neural Information Processing Systems*, pages 1660–1672, 2021.
- Paul Glasserman. *Monte Carlo Methods in Financial Engineering*. Springer, New York, 2004.
- Lawrence R. Glosten, Ravi Jagannathan, and David E. Runkle. On the relation between the expected value and the volatility of the nominal excess return on stocks. *Journal of Finance*, 48(5):1779–1801, 1993.
- James Pickands III. Statistical inference using extreme order statistics. *Annals of Statistics*, 3(1):119–131, 1975.
- Philippe Jorion. *Value-at-Risk: The New Benchmark for Managing Financial Risk*. McGraw-Hill, New York, 3 edition, 2007.
- J.P. Morgan/Reuters. Riskmetrics technical document. Technical report, 1996.
- Guolin Ke, Qi Meng, Thomas Finley, Taifeng Wang, Wei Chen, Weidong Ma, Qiwei Ye, and Tie-Yan Liu. LightGBM: A highly efficient gradient boosting decision tree. In *Advances in Neural Information Processing Systems*, pages 3146–3154, 2017.
- Roger Koenker and Gilbert Bassett. Regression quantiles. *Econometrica*, 46(1):33–50, 1978.
- Paul H. Kupiec. Techniques for verifying the accuracy of risk measurement models. *Journal of Derivatives*, 3(2):73–84, 1995.
- Harry Markowitz. Portfolio selection. *Journal of Finance*, 7(1):77–91, 1952.
- Mieszko Mazur, Mykola Dang, and Miguel Vega. Covid-19 and the march 2020 stock market crash: Evidence from s&p 1500. *Finance Research Letters*, 38:101690, 2021.
- Alexander J. McNeil and Rüdiger Frey. Estimation of tail-related risk measures for heteroscedastic financial time series: An extreme value approach. *Journal of Empirical Finance*, 7(3–4):271–300, 2000.

- Nicolai Meinshausen. Quantile regression forests. *Journal of Machine Learning Research*, 7: 983–999, 2006.
- Daniel B. Nelson. Conditional heteroskedasticity in asset returns: A new approach. *Econometrica*, 59(2):347–370, 1991.
- R. Tyrrell Rockafellar and Stanislav Uryasev. Optimization of conditional value-at-risk. *Journal of Risk*, 2(3):21–41, 2000.
- Kamile Stankeviciute, Ahmed M. Alaa, and Mihaela van der Schaar. Conformal time-series forecasting. In *Advances in Neural Information Processing Systems*, pages 6216–6228, 2021.
- James W. Taylor. A quantile regression neural network approach to estimating the conditional density of multiperiod returns. *Journal of Forecasting*, 19(4):299–311, 2000.
- Vladimir Vovk, Alexander Gammerman, and Glenn Shafer. *Algorithmic Learning in a Random World*. Springer, New York, 2005.
- Chen Xu and Yao Xie. Conformal prediction interval for dynamic time-series forecasting. In *Proceedings of the 38th International Conference on Machine Learning*, pages 11559–11569, 2021.

## A. MATHEMATICAL PROOFS

This section provides the proofs of Theorems 4.1 and 4.2.

### A.1 Proof of Finite-Sample Validity (Theorem 4.1)

**Theorem Statement.** Under exchangeability of the pairs  $\{(X_i, Y_i)\}_{i=1}^{n+1}$ , the conformal prediction set  $\Gamma_{1-\alpha}$  satisfies:

$$\Pr(Y_{n+1} \in \Gamma_{1-\alpha}(X_{n+1})) \geq 1 - \alpha.$$

**Proof.** Let the set of non-conformity scores be  $\mathcal{A} = \{\alpha_1, \dots, \alpha_n, \alpha_{n+1}\}$ , where  $\alpha_i = A(X_i, Y_i)$  for  $i = 1, \dots, n+1$ . The core assumption of exchangeability implies that any permutation of the sequence of pairs  $(X_1, Y_1), \dots, (X_{n+1}, Y_{n+1})$  is equally likely. Consequently, any permutation of the scores in  $\mathcal{A}$  is also equally likely.

This symmetry implies that the rank of the test score  $\alpha_{n+1}$  within the set  $\mathcal{A}$  is uniformly distributed on  $\{1, 2, \dots, n+1\}$ . Let us define the rank of  $\alpha_{n+1}$  as  $R_{n+1} = \sum_{i=1}^{n+1} \mathbf{1}(\alpha_i \leq \alpha_{n+1})$ . Due to exchangeability, we have  $\Pr(R_{n+1} = k) = \frac{1}{n+1}$  for any  $k \in \{1, \dots, n+1\}$ .

The conformal prediction set is defined as  $\Gamma_{1-\alpha}(X_{n+1}) = \{y : p(y) > \alpha\}$ , where the p-value  $p(y)$  is the fraction of scores greater than or equal to the score of the candidate point  $(X_{n+1}, y)$ . The true observation  $Y_{n+1}$  is excluded from this set if and only if its p-value is less than or equal to  $\alpha$ . The p-value for the true observation is  $p(Y_{n+1}) = \frac{1}{n+1} \sum_{i=1}^{n+1} \mathbf{1}(\alpha_i \geq \alpha_{n+1})$ .

The event of miscoverage,  $Y_{n+1} \notin \Gamma_{1-\alpha}(X_{n+1})$ , occurs if  $p(Y_{n+1}) \leq \alpha$ . This is equivalent to the rank of  $\alpha_{n+1}$  being “small.” Specifically,  $\frac{R_{n+1}}{n+1} \leq \alpha$ , which implies  $R_{n+1} \leq \lfloor \alpha(n+1) \rfloor$ .

We can now bound the probability of this miscoverage event:

$$\Pr(Y_{n+1} \notin \Gamma_{1-\alpha}(X_{n+1})) = \Pr(R_{n+1} \leq \lfloor \alpha(n+1) \rfloor) = \sum_{k=1}^{\lfloor \alpha(n+1) \rfloor} \Pr(R_{n+1} = k).$$

Since  $\Pr(R_{n+1} = k) = \frac{1}{n+1}$ , this sum is:

$$\sum_{k=1}^{\lfloor \alpha(n+1) \rfloor} \frac{1}{n+1} = \frac{\lfloor \alpha(n+1) \rfloor}{n+1} \leq \frac{\alpha(n+1)}{n+1} = \alpha.$$

Therefore, the probability of miscoverage is at most  $\alpha$ , which implies that the probability of correct coverage is at least  $1 - \alpha$ . This completes the proof. ■

## A.2 Proof of Asymptotic Calibration (Theorem 4.2)

**Theorem.** Under (A1)–(A4) and the update  $C_{t+1} = C_t + \gamma_t e_t$  with  $e_t = \mathbf{1}\{r_t \notin [\ell_t, u_t]\} - \alpha$ , we have  $C_t \rightarrow C^*$  a.s. where  $g(C^*) = 1 - \alpha$ , and  $\frac{1}{T} \sum_{t=1}^T \mathbf{1}\{r_t \in [\ell_t, u_t]\} \rightarrow 1 - \alpha$  a.s.

**Proof. Step 1 (Notation and stability).** Let  $\mathcal{F}_t$  be the filtration generated by the data up to time  $t$ . Define  $g(C) = \Pr(r_t \in [\ell_t, u_t] \mid C_t = C)$  and  $\phi(C) = \mathbb{E}[e_t \mid C_t = C] = \alpha - g(C)$ . By (A3),  $\phi$  is continuous and strictly decreasing in a neighborhood of its unique root  $C^*$  with  $\phi(C^*) = 0$ . Under (A1) the two-sided nonconformity scores are bounded, hence there exists  $S < \infty$  such that valid thresholds lie in  $[0, S]$ . Without loss of generality we assume the recursion is kept in a compact interval (e.g., via projection onto  $[0, S]$ ); this is standard in SA and does not change the produced intervals.

**Step 2 (SA decomposition).** Decompose the coverage error into signal + noise:

$$e_t = \mathbb{E}[e_t \mid \mathcal{F}_{t-1}] + \Delta_t = \phi(C_t) + \Delta_t,$$

where  $\Delta_t := e_t - \mathbb{E}[e_t \mid \mathcal{F}_{t-1}]$  is a martingale-difference sequence with  $\mathbb{E}[\Delta_t \mid \mathcal{F}_{t-1}] = 0$  and uniformly bounded second moments by (A2). The recursion becomes

$$C_{t+1} = C_t + \gamma_t \{\phi(C_t) + \Delta_t\}. \quad (3)$$

**Step 3 (Convergence of  $C_t$  to  $C^*$ ).** Consider the Lyapunov function  $V(c) = (c - C^*)^2$ . From (3),

$$C_{t+1} - C^* = (C_t - C^*) + \gamma_t \{\phi(C_t) + \Delta_t\},$$

hence

$$V(C_{t+1}) = (C_t - C^*)^2 + 2\gamma_t(C_t - C^*)\{\phi(C_t) + \Delta_t\} + \gamma_t^2\{\phi(C_t) + \Delta_t\}^2.$$

Taking conditional expectation and using  $\mathbb{E}[\Delta_t \mid \mathcal{F}_{t-1}] = 0$ ,

$$\mathbb{E}[V(C_{t+1}) \mid \mathcal{F}_{t-1}] = V(C_t) + 2\gamma_t(C_t - C^*)\phi(C_t) + \gamma_t^2 \mathbb{E}[\{\phi(C_t) + \Delta_t\}^2 \mid \mathcal{F}_{t-1}].$$

By (A1)–(A2) and compactness of the state space, there exists  $K < \infty$  with  $\mathbb{E}[(\phi(C_t) + \Delta_t)^2 \mid \mathcal{F}_{t-1}] \leq K$  a.s. By (A3),  $\phi$  is strictly decreasing near  $C^*$ , hence there exists  $\eta > 0$  and  $\rho > 0$  such that  $(C - C^*)\phi(C) \leq -\eta(C - C^*)^2$  whenever  $|C - C^*| \leq \rho$ . Since iterates remain in a compact interval and step-sizes decrease, standard SA stability (together with projection if used) ensures that eventually  $|C_t - C^*| \leq \rho$  a.s. (alternatively, one may argue by contradiction using the drift term). Therefore, for all large  $t$ ,

$$\mathbb{E}[V(C_{t+1}) \mid \mathcal{F}_{t-1}] \leq V(C_t) - 2\eta\gamma_t(C_t - C^*)^2 + K\gamma_t^2.$$

By the Robbins–Siegmund supermartingale convergence lemma, since  $\sum_t \gamma_t^2 < \infty$  and  $V(\cdot) \geq 0$ , we obtain that  $V(C_t)$  converges a.s. and  $\sum_t \gamma_t(C_t - C^*)^2 < \infty$  a.s. Because  $\sum_t \gamma_t = \infty$  (A4),

the latter implies  $\liminf_t (C_t - C^*)^2 = 0$ , and together with the monotone drift near  $C^*$  yields  $C_t \rightarrow C^*$  almost surely.

**Step 4 (Time-average calibration).** Recall  $e_t = \phi(C_t) + \Delta_t$ . Since  $C_t \rightarrow C^*$  and  $\phi$  is continuous,  $\phi(C_t) \rightarrow 0$  a.s.; by Cesàro averaging,  $\frac{1}{T} \sum_{t=1}^T \phi(C_t) \rightarrow 0$  a.s. By (A2) and square-integrability of  $\Delta_t$ , the strong law for martingale differences (e.g., Hall & Heyde, 1980) implies  $\frac{1}{T} \sum_{t=1}^T \Delta_t \rightarrow 0$  a.s. Hence

$$\frac{1}{T} \sum_{t=1}^T e_t = \frac{1}{T} \sum_{t=1}^T \phi(C_t) + \frac{1}{T} \sum_{t=1}^T \Delta_t \xrightarrow{\text{a.s.}} 0.$$

Equivalently,  $\frac{1}{T} \sum_{t=1}^T \mathbf{1}\{r_t \in [\ell_t, u_t]\} \rightarrow 1 - \alpha$  a.s., which completes the proof. ■

## B. SUPPLEMENTARY VISUALIZATIONS

This section provides the prediction interval visualizations for BTC-USD (3) and Gold (4) during the COVID-19 market crash (February-April 2020).

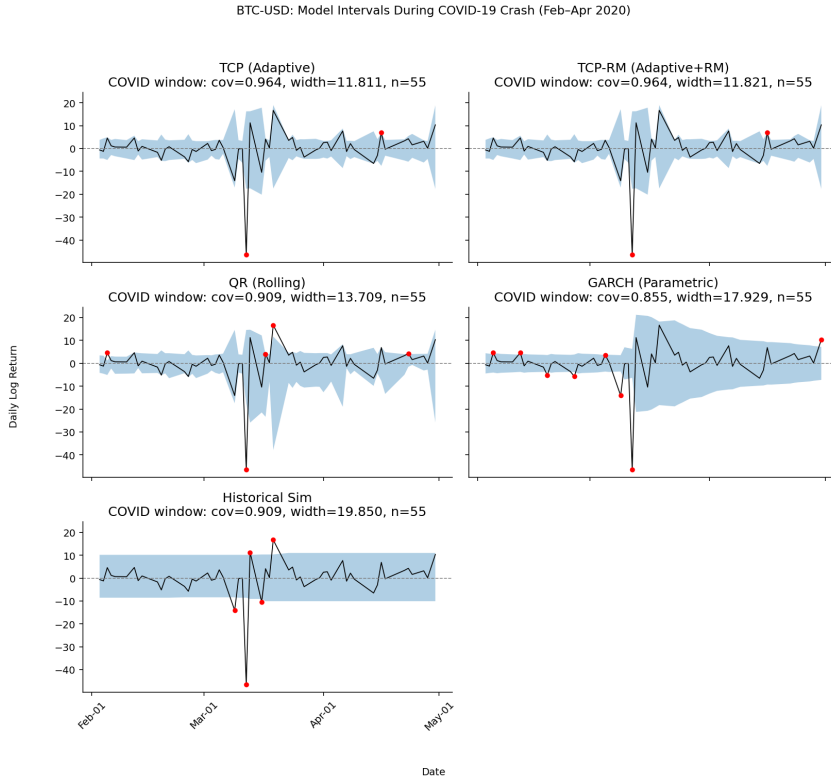


Figure 3: A comparison of 95% prediction intervals from all four models for BTC-USD daily returns during the COVID-19 market crash (February-April 2020).

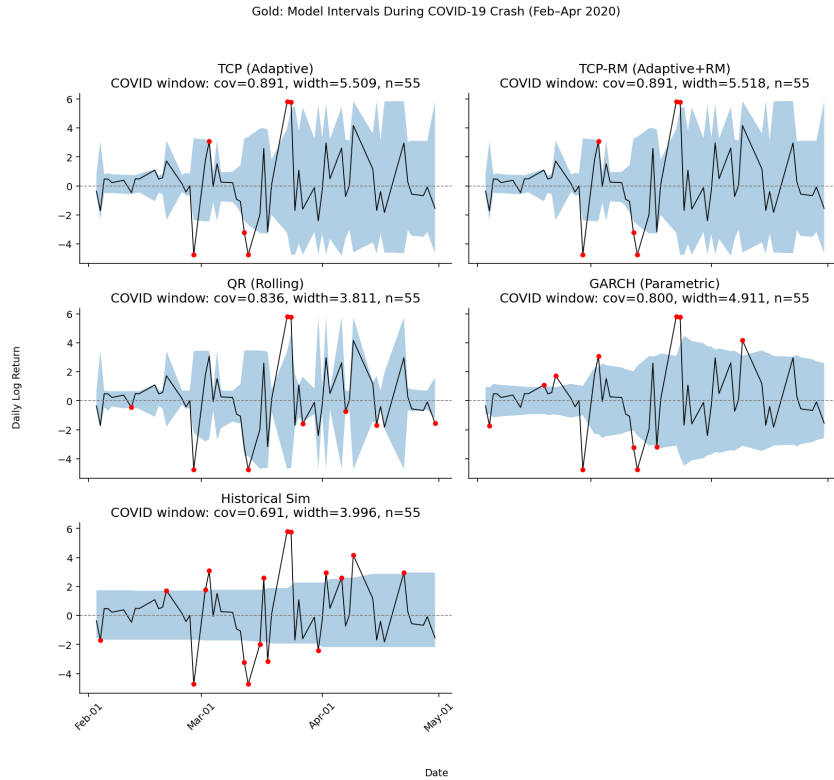


Figure 4: A comparison of 95% prediction intervals from all four models for Gold daily returns during the COVID-19 market crash (February-April 2020).

## C. VISUALIZATIONS OF THE TCP VS TCP-RM TRACE PLOTS

This section provides the visualizations of the TCP vs TCP-RM trace plots for BTC-USD (Figure 5) and Gold (Figure 6), complementing the main visualization for the S&P 500 presented in the results section.

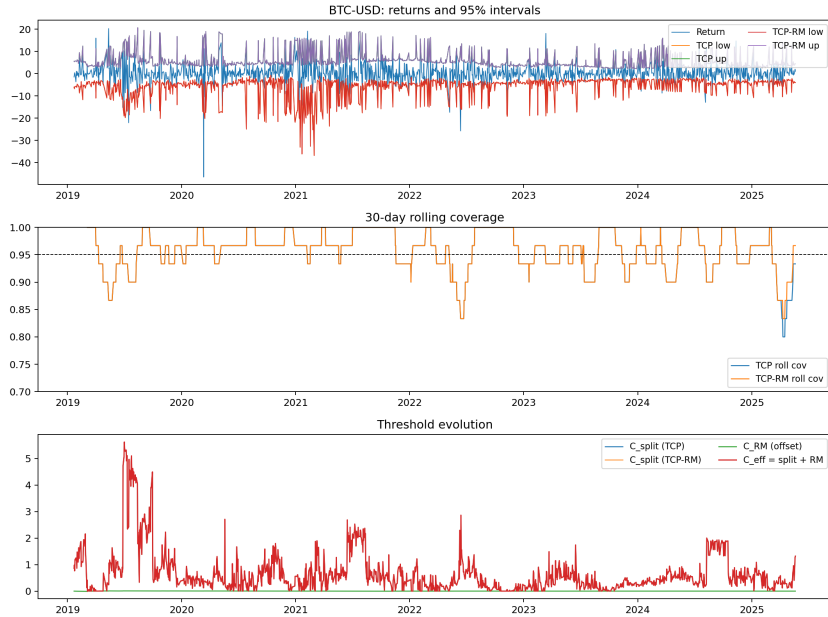


Figure 5: **TCP vs. TCP-RM on BTC-USD (95% intervals)**. Same layout as Fig. 2. Large, frequent shocks lead to sustained but controlled elevations in  $C_{\text{eff}}$ , keeping rolling coverage close to 95% while allowing intervals to shrink as volatility recedes.

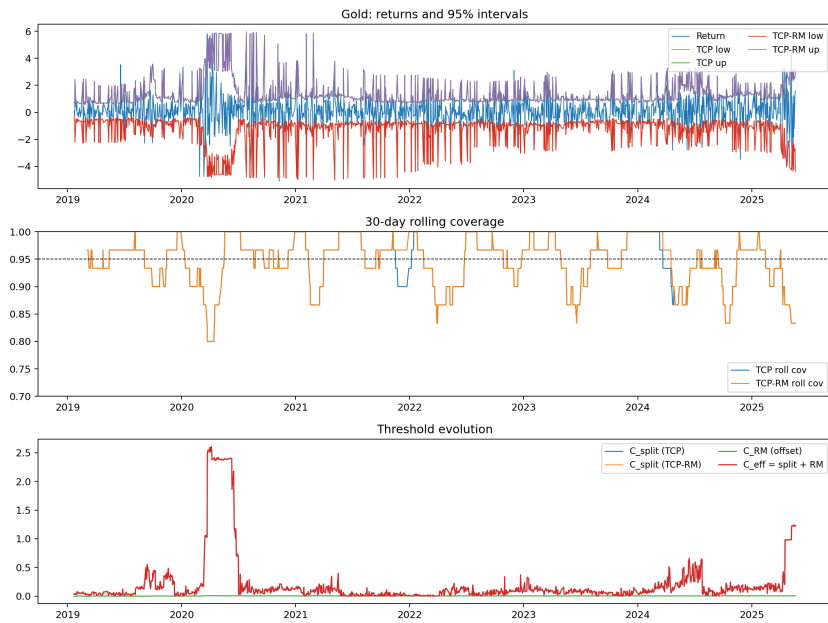


Figure 6: **TCP vs. TCP-RM on Gold (95% intervals)**. Same layout as Fig. 2. Spikes in  $C_{\text{eff}}$  are concentrated around crisis windows; elsewhere,  $C_{\text{RM}}$  stays near zero and the method behaves like standard split-conformal TCP.

## D. SUPPLEMENTARY SENSITIVITY ANALYSIS

This section provides the full sensitivity analysis results for BTC-USD (Table 3) and Gold (Table 4), complementing the main analysis on the S&P 500 presented in the results section. The findings confirm that the TCP-RM framework is robust and performs consistently across different asset classes and hyperparameter settings.

Table 3: TCP-RM sensitivity on **BTC-USD** with  $|\mathcal{C}| = 40$ .

Hyperparameters		Performance	
Window Size ( $w$ )	$\gamma_0$	Coverage	Interval Width
100	0.005	0.9519	17.1883
100	0.010	0.9519	17.1899
100	0.050	0.9519	17.2031
252	0.005	0.9593	10.7970
252	0.010	0.9593	10.7974
252	0.050	0.9593	10.8004
500	0.005	0.9517	9.0519
500	0.010	0.9525	9.0544
500	0.050	0.9542	9.0737

Table 4: TCP-RM sensitivity on **Gold** with  $|\mathcal{C}| = 40$ .

Hyperparameters		Performance	
Window Size ( $w$ )	$\gamma_0$	Coverage	Interval Width
100	0.005	0.9538	3.7060
100	0.010	0.9532	3.7066
100	0.050	0.9532	3.7109
252	0.005	0.9517	2.6241
252	0.010	0.9524	2.6245
252	0.050	0.9524	2.6294
500	0.005	0.9534	2.4083
500	0.010	0.9609	2.4212
500	0.050	0.9542	2.4105

## E. SUPPLEMENTARY SENSITIVITY ANALYSIS ON TCP (NO RM)

For completeness, in Tables 5, 6 and 7, we also report sensitivity for **TCP** (split-conformal only, no Robbins–Monro offset). We vary  $w \in \{100, 252, 500\}$  with  $|\mathcal{C}| = 40$  for each asset.

Table 5: TCP sensitivity on **S&P 500** with  $|\mathcal{C}| = 40$ .

Window Size ( $w$ )	Coverage	Interval Width
100	0.9557	4.5174
252	0.9455	3.4538
500	0.9450	3.2376

Table 6: TCP sensitivity on **BTC-USD** with  $|\mathcal{C}| = 40$ .

Window Size ( $w$ )	Coverage	Interval Width
100	0.9519	17.1866
252	0.9593	10.7967
500	0.9500	9.0469

Table 7: TCP sensitivity on **Gold** with  $|\mathcal{C}| = 40$ .

Window Size ( $w$ )	Coverage	Interval Width
100	0.9538	3.7055
252	0.9517	2.6234
500	0.9417	2.3872

As with TCP-RM, larger  $w$  generally yields narrower intervals. Without the adaptive offset, coverage can dip slightly below 95% in some settings, underscoring the benefit of the online calibration layer.